RESEARCH ARTICLE

Vacuum Ultraviolet Photodetector with Low Dark Current and Fast Response Speed Based on Polycrystalline AlN Thin Film

Peixuan Zhang, Kewei Liu, Yongxue Zhu, Qiu Ai, Jialin Yang, Xing Chen, Zhen Cheng, Binghui Li, Lei Liu, and Dezhen Shen**

A metal–semiconductor–metal (MSM) vacuum ultraviolet (VUV) photodetector is realized on polycrystalline AlN film grown by molecular beam epitaxy. At a bias of 10 V, the dark current of the device is less than 120 fA and the VUV (185 nm) to Ultraviolet-C (255 nm) rejection ratio is more than 10^3. More interestingly, the polycrystalline AlN photodetector shows an ultra-fast response speed with a 90%–10% decay time of $\approx$50 ns, which is much quicker than any other previously reported AlN VUV photodetectors. Furthermore, the device still maintains stability and repeatability at 473 K. This research shows that polycrystalline AlN photodetector has good photodetection performance, which will help advance the design and preparation of AlN-based VUV photodetectors.

1. Introduction

Vacuum ultraviolet (VUV, 120–200 nm) photodetectors have attracted great interest in recent years, due to their potential application such as securing space communications, studying the expansion and elements of nebulas, probing the formation and evolution of solar storms and so on.[1–7] Wide bandgap semiconductors (such as GaN, Ga_2O_3, and ZnO) have been considered ideal candidates for UV photodetectors.[8–14] However, the reported photodetectors based on wide bandgap semiconductors cannot meet the accurate detection of light shorter than 200 nm due to the relatively narrow bandgaps (<5 eV). AlN is a potential material for highly selective VUV photodetection because it has a relatively wide bandgap of $\approx$6.2 eV at room temperature. In addition, AlN also has the advantages of good

chemical stability, high mobility, fast saturation speed, high breakdown field strength, and high radiation hardness, making it an excellent candidate material for VUV photodetectors.[15–17] In the past two decades, AlN-based VUV photodetectors have made remarkable progress.[18–28] In 2006, Jiang et al. reported AlN deep ultraviolet (DUV) photodetectors with metal–semiconductor–metal (MSM) structure, and the device has a sharp cutoff wavelength at 207 nm and exhibits a peak response at 200 nm.[18] After that, a two-step physical vapor transport method was employed by Zheng et al. to fabricate AlN micro/nanowire VUV photodetectors with a VUV/UV suppression ratio $>10^2$ and a response time of <0.2 s.[22] To improve the responsivity and response speed of the AlN VUV photodetector, a flip-chip 3D MSM device was designed and fabricated, and the enhanced performance was attributed to the intensified electric field.[24]

To date, almost all the reported AlN VUV photodetectors are based on high-quality single crystalline films or micro/nanostructures, which commonly require harsh fabrication conditions (i.e., homoepitaxial growth at high temperatures). Compared with single crystalline materials, polycrystalline or amorphous materials have the advantages of low growth temperature, simple growth process, large wafer size, and low cost, which have attracted widespread attention. Moreover, the grain boundaries in the polycrystalline structure have an important influence on the transport of carriers, and can further affect the photodetection performance of the materials.[29–31] Amazingly, the photodetectors based on Si and Ga_2O_3 polycrystalline materials have demonstrated great advantages in dark current and response speed.[32,33] However, no information can be found about the photodetectors based on polycrystalline AlN.

In this work, plasma-assisted molecular beam epitaxy (P-MBE) was used to grow polycrystalline AlN thin films on *c*-plane sapphire substrates at a low temperature, and a polycrystalline AlN MSM VUV photodetector was fabricated by standard photolithography and lift-off processes. At room temperature, the dark current of the polycrystalline AlN photodetector is less than 120 fA at 10 V bias and the VUV/Ultraviolet-C (UVC) rejection ratio exceeds 10^3. In addition, the device shows an ultrafast response speed and a decay time of just 50 ns, which is more than two orders of magnitude faster than the previously reported

P. Zhang, K. Liu, Y. Zhu, Q. Ai, J. Yang, X. Chen, Z. Cheng, B. Li, L. Liu, D. Shen
State Key Laboratory of Luminescence and Applications
Changchun Institute of Optics
Fine Mechanics and Physics
Chinese Academy of Sciences
Changchun 130033, China
E-mail: liukw@ciomp.ac.cn; shendz@ciomp.ac.cn

P. Zhang, K. Liu, Y. Zhu, Q. Ai, J. Yang, X. Chen, Z. Cheng, B. Li, L. Liu, D. Shen
Center of Materials Science and Optoelectronics Engineering
University of Chinese Academy of Sciences
Beijing 100049, China

AlN VUV photodetectors. In addition, at 473 K, the polycrystalline AlN photodetector still exhibits photoresponse performance with good repeatability and stability. A feasible way of realizing high-performance VUV photodetectors is presented in this study.

2. Results and Discussion

Reflection high-energy electron diffraction was used for in situ detection in the process of AlN film growth. As shown in **Figure 1**a, the reflective high energy electron diffraction (RHEED) pattern shows rings, indicating that polycrystalline AlN was grown on the sapphire substrate. This phenomenon is caused by the large lattice mismatch between the AlN and c-plane sapphire substrate.[34] The X-ray diffraction (XRD) test was carried out on the polycrystalline AlN film to further understand the structural characteristics of the polycrystalline AlN film. As shown in Figure 1b, only a weak (0002) diffraction peak was observed except for the diffraction peaks of the sapphire substrate, which proves that the AlN film is a mixture of amorphous and polycrystalline. In addition, we calculated the grain size of polycrystalline aluminum nitride films using the Debye–Scherrer formula

$$D = \frac{K\gamma}{B\cos\theta} \tag{1}$$

Here, D is the average thickness of grains perpendicular to the crystal plane, K is Scherrer constant, γ is the X-ray wavelength, B is the half-width of the diffraction peak of the measured sample, θ is Bragg diffraction angle. The average grain size of polycrystalline aluminum nitride thin films calculated is about 12.5 nm.

Figure 2a shows the transmission spectrum of polycrystalline AlN film grown on the c-plane sapphire substrate. Substrate contribution not included. The prepared polycrystalline AlN film has a transmittance of more than 90% at wavelengths greater than 250 nm. As shown in the inset of Figure 2a, it can be concluded that the bandgap of polycrystalline AlN is about 6.03 eV from the Tauc plot. The top view and cross-sectional SEM images of the polycrystalline AlN film are shown in Figure 2b, and it can be seen that the polycrystalline AlN film has a thickness of about 120 nm with a uniform and smooth plane. As shown in Figure 2c, the atomic force microscopy (AFM) image reveals that the surface of the AlN film is very flat, and the root mean square (RMS) roughness in a scanned area of $1 \, \mu m^2$ is about 2 nm.

To investigate the optoelectronic properties of polycrystalline AlN film, Au interdigitated electrodes were fabricated on the film. **Figure 3**a depicts the I–V characteristic curves of the polycrystalline AlN photodetector under 185 nm (6.7 eV, average power of 70 μW cm^{-2}) and 255 nm (4.9 eV, average power of 7 mW cm^{-2}) UV light illuminations and in the dark state. When the applied bias voltage is 10 V, the dark current of the device is ≈120 fA (instrumental limit), while the photocurrent
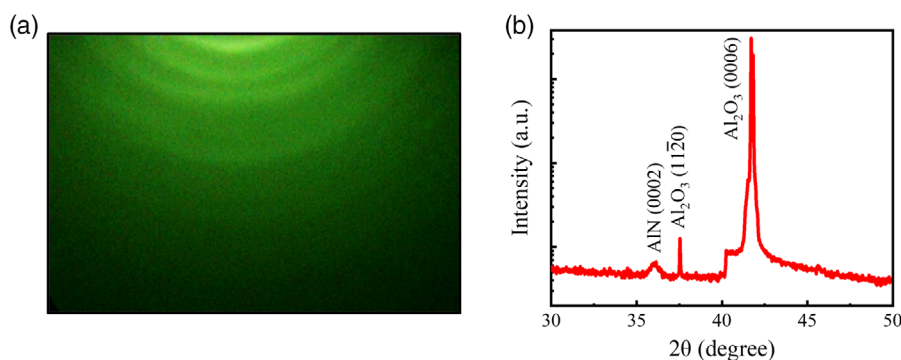

Figure 1. a) RHEED pattern of the AlN film grown at 600 °C. b) X-ray diffraction (XRD) pattern of the polycrystalline AlN film.
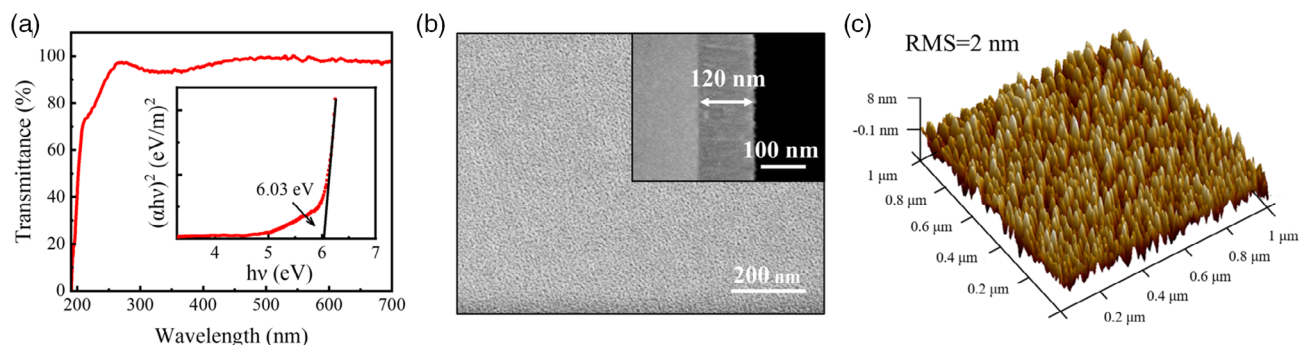

Figure 2. a) Room-temperature absorption spectra of polycrystalline AlN films at wavelengths of 190–700 nm. The inset shows the variation of $(\alpha h\nu)^2$ versus the photo energy ($h\nu$). b) Top view and cross-sectional (inset) scanning electron microscope (SEM) images of polycrystalline AlN. c) AFM image of the polycrystalline AlN surface in a scanned area of $1 \, \mu m^2$.
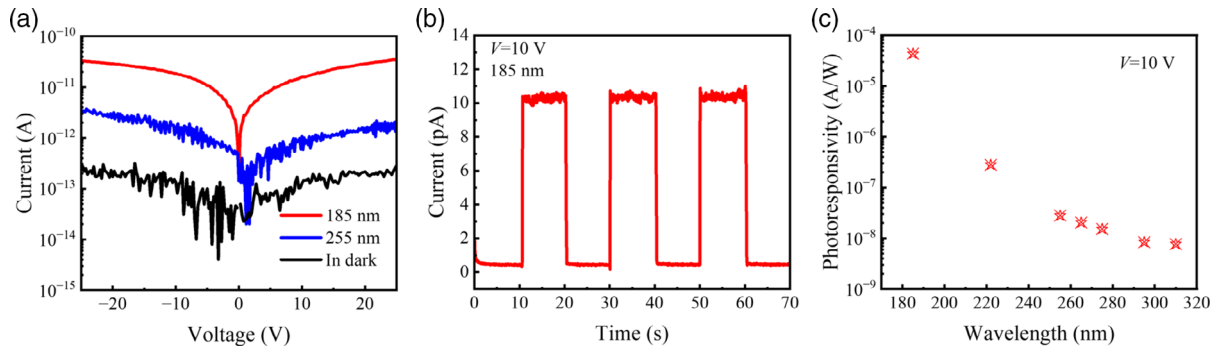
Figure 3. a) Under 185 nm (with an average power density of 70 µW cm^{-2}) and 255 nm (with an average power density of 7 mW cm^{-2}) light illuminations and in the dark state, the I–V characteristic curves of the polycrystalline AlN photodetector. b) Time-dependent photocurrent of the photodetector by periodically switching ON/OFF 185 nm lamp illumination under 10 V bias. c) The responsivity is a function of wavelength.

is 15 pA and 1.1 pA to the illumination of 185 and 255 nm, respectively. As shown in Figure S1, Supporting Information, the polycrystalline AlN photodetector still has a low dark current at 100 V, and there is no breakdown phenomenon. Figure 3b shows the time-dependent response of the device under 185 nm lamp illumination at 10 V bias. The 185 nm lamp was periodically switched ON/OFF every 10 s. It can be seen that the prepared AlN photodetector in this work shows good repeatability, excellent stability, and fast response speed. Responsivity (R) is an important parameter for the photodetectors and it can be calculated by the following equation

$$R = \frac{I_{light} - I_{dark}}{p_{opt} \cdot S} \quad (2)$$

where I_{light} is the current under illumination, I_{dark} is the current in dark, p_{opt} is the illumination intensity, and S is the efficient area.[35] Our polycrystalline AlN photodetector exhibits a responsivity of 43 µA W^{-1} at 185 nm and 28 nA W^{-1} at 255 nm. And the responsivity as a function of the illumination wavelength is shown in Figure 3c. The VUV/UVC rejection ratio ($R_{185\,nm}/R_{255\,nm}$) can reach as high as more than 10^3. In addition, the specific detectivity (D^*) can be calculated to be 4.9×10^{10} cm Hz$^{1/2}$ W^{-1} (Jones) at 185 nm using the following equation[36]

$$D^* = \frac{R}{\sqrt{2qI_{dark}/S}} \quad (3)$$

where q is the free electron charge of 1.6×10^{-19} C.

Meanwhile, thermal stability is also very important for the practical applications of photodetectors, especially in the high-temperature operating environment. To investigate the photoresponse characteristic of the device at high temperature, the polycrystalline AlN photodetector was placed on a hot plate in an air atmosphere. As shown in **Figure 4**a, almost linear dark J–V curves can be clearly obtained at 323, 373, 423, and 473 K, indicating the good ohmic contacts between the Au electrode and AlN film at all test temperatures. In addition, the dark current destiny showed a significant increase with the increase in temperature. Figure 4b presents the dark current destiny of the device as a function of the temperature at 10 V bias. It can be seen that there is an exponential relationship between dark current density and temperature due to the thermal excitation of carriers in polycrystalline AlN film. In addition, when the bias voltage is 10 V, the time-dependent photoresponse characteristics of the device were tested by periodically switching ON/OFF the 185 nm lamp at 323, 373, 423, and 473 K. (see Figure 4c). As the temperature increases, the dark current density of the device increases significantly, while the photocurrent density also increases slightly. The increase in photocurrent density with increasing the temperature should be associated with the enhanced
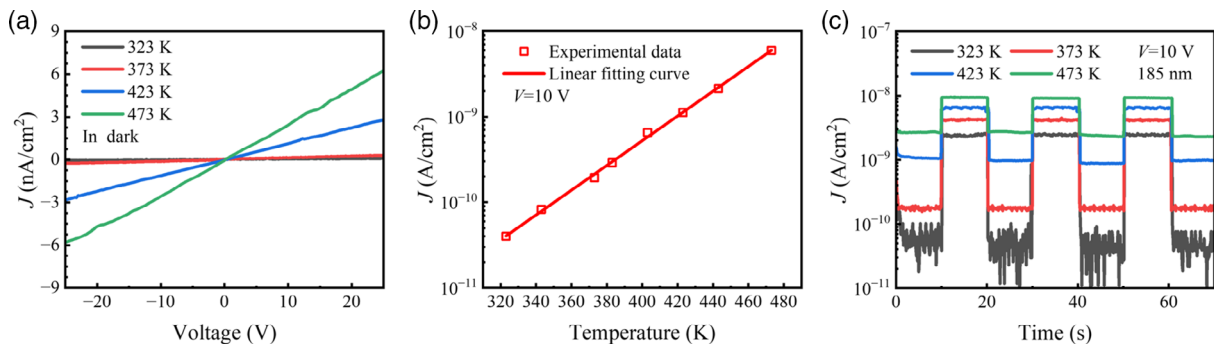

Figure 4. a) At 323, 373, 423, and 473 K, the J–V characteristic curves of polycrystalline AlN photodetector in dark state. b) Dark current density as a function of temperature. c) The time-dependent photocurrent density of the photodetector at different temperatures.
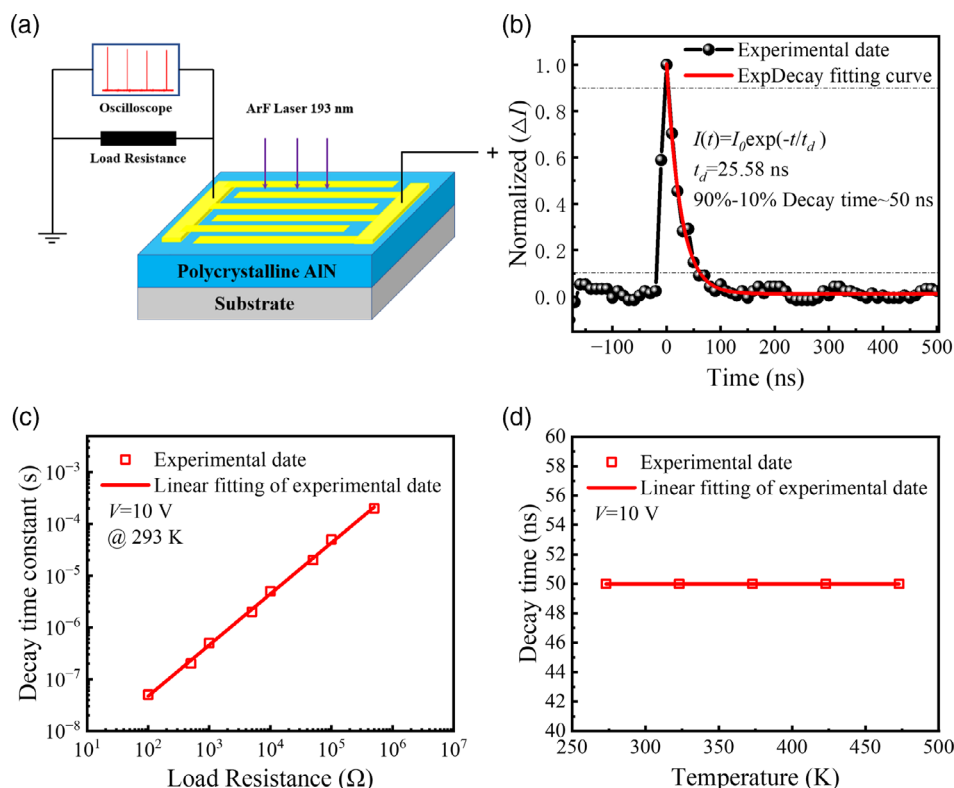
Figure 5. a) The schematic diagram of our experimental setup for measuring the temporal-response of polycrystalline AlN photodetector. b) Relationship between temporal-dependent response (ns) and normalized ΔI. c) The dependence of decay time constant on load resistance. d) Transient response speed of polycrystalline AlN detector as a function of operating temperature.

absorption of AlN at elevated temperature, which in turn leads to the absorption of more photons emitted by the 185 nm lamp.[37–40] After turning off the light, the device can quickly recover the initial value in the dark state at all temperatures.

The temporal-dependent response of the polycrystalline AlN photodetector was studied using a pulsed ArF excimer laser with a wavelength of 193 nm (laser pulse width of 10 ns, frequency of 10 Hz) and a high-speed digital oscilloscope. **Figure 5**a is a schematic diagram of the experimental setup for response time measurement. A single normalized photoresponse was shown in Figure 5b with a load resistance of 100 Ω. The decay edge can be well-fitted by a single exponential function as

$$I(t) = I_0\exp\left(\frac{-t}{t_d}\right) \tag{4}$$

where I_0 is the peak photocurrent, t is the time, and t_d is the decay time constant. The decay time constant can be estimated to be 25.58 ns from the fitting result. The response time is defined as the time interval between 10%–90% of amplitudes. As shown in Figure 5b, the 90%–10% decay time for polycrystalline AlN photodetector is around 50 ns, which is significantly shorter than those of the previously reported AlN DUV photodetectors.

The relationship between decay time and load resistance of the device was tested by using different resistances. As shown in Figure 5c, the decay time of polycrystalline AlN MSM photodetector linearly increases with the increasing load resistance. This

trend implies that the response speed is limited by the RC constants in the exponential regime, where R is the load resistance and C is the sum of the capacitance of the device and the load capacitance of our measurement system. As shown in Figure 5d, the temporal-dependent response of the device was tested at different temperatures. It can be clearly seen that the response speed of the device hardly changes as the operating temperature increases.

Table 1 summarizes the dark current, responsivity, VUV/UVC rejection ratio, response time of the reported AlN photodetectors. The VUV/UVC rejection ratio and the dark current of polycrystalline AlN MSM photodetector are better than that of most previously reported devices. Most importantly, the polycrystalline AlN MSM photodetector has the fastest response speed. As is well known, the grain boundary barrier in the polycrystalline structure has an important influence on the transport of carriers. Therefore, a large number of grain boundaries in polycrystalline AlN should be the main reason for the low dark current and fast response speed of the AlN photodetector in this work.

3. Conclusion

In summary, polycrystalline AlN film was fabricated on a *c*-face sapphire substrate by MBE at a low temperature of 600 °C. And an MSM photodetector was demonstrated on polycrystalline AlN film, which shows a low dark current (<120 fA at 10 V) and an

Table 1. Dark current, photoresponsivity, rejection ratio of VUV/UVC, response time for typical semiconductor-based VUV photodetectors.

Materials	Dark current [A]	VUV light [nm]	Bias [V]	Photoresponsivity [mA W^{-1}]	Rejection ratio of VUV/UVC	Decay time [s]	Ref.
AlN	5×10^{-14}@30 V	190	30	4.5	$\approx 10^4$	<3	[19]
AlN	6×10^{-9}@8 V	200	5	0.6	–	1.8	[23]
AlN	10^{-9}@10 V	200	2	10	–	$<8 \times 10^{-3}$	[24]
p-Gr/AlN/n-SiC	10^{-10}@4 V	194	3	79	$\approx 10^4$	5×10^{-6}	[6]
p-Gr/AlN	10^{-8}@1 V	195	0	67	$\approx 10^3$	4×10^{-4}	[41]
p-Gr/AlN/n-ZnO	10^{-8}@2 V	185	0	40	$\approx 10^2$	1×10^{-3}	[42]
AlN	5×10^{-14}@10 V	185	10	6.44	$\approx 10^3$	3.6	[43]
Polycrystalline AlN	1.2×10^{-13}@10 V	185	10	0.043	$\approx 10^3$	5×10^{-8}	This work

ultrafast response speed. Notably, the 90%–10% decay time of ≈50 ns, which is two orders of magnitude faster than the previously reported AlN VUV photoconductive detectors. Moreover, the device has excellent spectral selectivity, and the VUV/UVC rejection ratio exceeds 10^3. The grain boundaries in polycrystalline AlN film can be responsible for the low dark current and fast response speed. In addition, as the temperature increases from 293 to 473 K, the device still maintains good and reliable VUV photodetection performance. The findings in this work provide a possibility for detecting VUV light in harsh environments.

4. Experimental Section

P-MBE was used to grow polycrystalline AlN film on the *c*-plane sapphire substrate. For the precursors, 6N-purity N$_2$ activated using an radio frequency plasma source was chosen as well as 6N-purity Al obtained from a standard Knudsen effusion cell. An ultrasonic bath was used to clean the sapphire substrate in trichloroethylene, acetone, alcohol, and deionized water prior to growth, and finally dried with high-purity N$_2$. After that, the substrate was pretreated at 700 °C for 2 h to remove the surface impurities. Polycrystalline AlN layer growth on sapphire substrates at 600 °C for 1 h. During the deposition process, the chamber was maintained in a high vacuum of 1×10^{-6} Torr and an N$_2$ flow rate of 1.1 sccm was used with a radio frequency power of 350 W. The crystalline quality of the samples was assessed using the X-ray diffractometer (XRD) with Cu Kα radiation ($\lambda = 0.154178$ nm). The surface and thickness of the AlN films were measured by SEM (Hitachi S-4800). The optical transmission and absorption spectra were recorded using a Shimadzu UV-3101PC scanning spectrophotometer. The surface morphology of samples was measured by AFM measurement was used to study.

With the approach of standard photolithography and lift-off processes, 25 pairs of Au (50 nm thick) interdigitated with a width of 10 μm, a length of 500 μm, and a spacing of 10 μm were prepared. Using a semiconductor device analyzer (Agilent B1500A), 185 nm lamp (ZW21D15W/Y), and 255 nm emitting diode (UVC3525 LED lamp), the current–voltage (*I–V*) properties and time-dependent photocurrent (*I–t*) properties of the device were measured at different temperatures. Measurements of temporal-dependent responses were performed using an ArF excimer laser (CL-5100, 193 nm) and oscilloscope (Tektronix DPO 5104 digital oscilloscope).

Supporting Information

Supporting Information is available from the Wiley Online Library or from the author.

Conflict of Interest

The authors declare no conflict of interest.

Data Availability Statement

The data that support the findings of this study are available from the corresponding author upon reasonable request.

[1] D. N. Baker, *Science* **2002**, *297*, 1486.
[2] D. N. Baker, S. G. Kanekal, X. Li, S. P. Monk, J. Goldstein, J. L. Burch, *Nature* **2004**, *432*, 878.
[3] H. Li, Y. Yang, J. Ren, Z. Zhou, X. Li, Y. Liu, J. Feng, *J. Environ. Chem. Eng.* **2022**, *10*, 107417.
[4] M. A. Guerrero, O. De Marco, *Astron. Astrophys.* **2013**, *553*, A126.
[5] O. Venot, Y. Bénilan, N. Fray, M. C. Gazeau, F. Lefèvre, *Astron. Astrophys.* **2018**, *609*, A34.
[6] W. Zheng, L. Jia, F. Huang, *iScience* **2020**, *23*, 101145.
[7] L. Jia, W. Zheng, F. Huang, *PhotoniX* **2020**, *1*, 1.
[8] A. Osinsky, S. Gangopadhyay, R. Gaska, B. Williams, M. A. Khan, D. Kuksenkov, H. Temkin, *Appl. Phys. Lett.* **1997**, *71*, 2334.
[9] B. S. Qiao, Z. Z. Zhang, X. H. Xie, B. H. Li, K. Li, X. Chen, H. Zhao, K. W. Liu, L. Liu, D. Z. Shen, *J. Phys. Chem. C* **2019**, *123*, 18516.
[10] K. W. Liu, J. G. Ma, J. Y. Zhang, Y. Lu, D. Y. Jiang, B. H. Li, D. Y. Zhao, Z. Z. Zhang, B. Yao, D. Z. Shen, *Solid-State Electron.* **2007**, *51*, 757.

[11] Q. Cai, H. You, H. Guo, J. Wang, B. Liu, Z. Xie, D. Chen, H. Lu, Y. Zheng, R. Zhang, *Light Sci Appl.* **2021**, *10*, 94.

[12] M. M. Fan, K. W. Liu, Z. Z. Zhang, B. H. Li, X. Chen, D. X. Zhao, C. X. Shan, D. Z. Shen, *Appl. Phys. Lette.* **2014**, *105*, 011117.

[13] Y. X. Zhu, K. W. Liu, Q. Ai, Q. C. Hou, X. Chen, Z. Z. Zhang, X. H. Xie, B. H. Li, D. Z. Shen, *J. Mater. Chem. C* **2020**, *8*, 2719.

[14] J. Hu, K. Liu, T. Ma, Y. Wei, J. Chen, Z. Li, *Opt. Laser Technol.* **2021**, *140*, 106946.

[15] Y. Taniyasu, M. Kasu, T. Makimoto, *Nature* **2006**, *441*, 325.

[16] L. Guo, Z. Hu, R. Wan, L. Long, T. Li, J. Yan, Y. Lin, L. Zhang, W. Zhu, L. Wang, *Nanophotonics* **2018**, *8*, 171.

[17] M. Bickermann, A. Münch, B. M. Epelbaum, O. Filip, P. Heimann, S. Nagata, A. Winnacker, *J. Appl. Phys.* **2008**, *103*, 073522.

[18] J. Li, Z. Y. Fan, R. Dahal, M. L. Nakarmi, J. Y. Lin, H. X. Jiang, *Appl. Phys. Lett.* **2006**, *89*, 213510.

[19] A. BenMoussa, J. F. Hochedez, R. Dahal, J. Li, J. Y. Lin, H. X. Jiang, A. Soltani, J. C. De Jaeger, U. Kroth, M. Richter, *Appl. Phys. Lette.* **2008**, *92*, 022108.

[20] S. Nikishin, B. Borisov, M. Pandikunta, R. Dahal, J. Y. Lin, H. X. Jiang, H. Harris, M. Holtz, *Appl. Phys. Lett.* **2009**, *95*, 054101.

[21] A. BenMoussa, A. Soltani, J. C. Gerbedoen, T. Saito, S. Averin, S. Gissot, B. Giordanengo, G. Berger, U. Kroth, J. C. De Jaeger, A. Gottwald, *Nucl. Instrum. Methods Phys. Res. Sect. B* **2013**, *312*, 48.

[22] W. Zheng, F. Huang, R. Zheng, H. Wu, *Adv. Mater.* **2015**, *27*, 3921.

[23] S. Kaushik, T. R. Naik, A. Alka, M. Garg, B. R. Tak, M. Ravikanth, V. R. Rao, R. Singh, *ACS Appl. Electron. Mater.* **2020**, *2*, 739.

[24] T. Li, L. Long, Z. Hu, R. Wan, X. Gong, L. Zhang, Y. Yuan, J. Yan, W. Zhu, L. Wang, J. Li, *Opt. Lett.* **2020**, *45*, 3325.

[25] L. Jia, W. Zheng, F. Huang, *ACS Photonics* **2022**, *9*, 2101.

[26] L. Jia, W. Zheng, R. Lin, F. Huang, *iScience* **2020**, *23*, 100818.

[27] M. Dong, W. Zheng, C. Xu, R. Lin, D. Zhang, Z. Zhang, F. Huang, *Adv. Opt. Mater.* **2019**, *7*, 1801272.

[28] W. Zheng, R. Lin, J. Ran, Z. Zhang, X. Ji, F. Huang, *ACS Nano* **2018**, *12*, 425.

[29] I. Shalish, L. Kronik, G. Segal, Y. Shapira, S. Zamir, B. Meyler, J. Salzman, *Phys. Rev. B* **2000**, *61*, 15573.

[30] D. Kim, K. M. Song, U. Jung, S. Kim, D. S. Shin, J. Park, *Appl. Sci.* **2020**, *10*, 1514.

[31] A. E. Wickenden, D. D. Koleske, R. L. Henry, R. J. Gorman, M. E. Twigg, M. Fatemi, J. A. Freitas, W. J. Moore, *J. Electron. Mater.* **2000**, *29*, 21.

[32] S. Yoon, K. Kim, H. Cho, J.-S. Yoon, M. J. Lee, M. Meyyappan, C. K. Baek, *Opt. Express* **2017**, *2*, 32910.

[33] C. Zhou, K. Liu, X. Chen, J. Feng, J. Yang, Z. Zhang, L. Liu, Y. Xia, D. Shen, *J. Alloys Compd.* **2020**, *840*, 155585.

[34] S. Inoue, K. Okamoto, T. Nakano, H. Fujioka, *J. Cryst. Growth* **2006**, *297*, 317.

[35] C. Li, H. Wang, F. Wang, T. Li, M. Xu, H. Wang, Z. Wang, X. Zhan, W. Hu, L. Shen, *Light Sci. Appl.* **2020**, *9*, 1.

[36] X. Luo, S. Chen, L. Liu, J. Lv, A. Qadir, K. Shehzad, X. Fan, *J. Phys. Chem. C* **2018**, *123*, 810.

[37] X. Tang, F. Ji, H. Wang, Z. Jin, H. Li, B. Li, J. Wang, *Appl. Phys. Lett.* **2021**, *119*, 013503.

[38] C. H. Su, W. Palosz, S. Zhu, S. L. Lehoczky, I. Grzegory, P. Perlin, T. Suski, *J. Cryst. Growth* **2002**, *235*, 111.

[39] Y. Ueda, S. Akita, Y. Nomura, Y. Nakayama, H. Naito, *Thin Solid Films* **2008**, *517*, 1471.

[40] B. R. Tak, M. Garg, S. Dewan, C. G. Torres-Castanedo, K. H. Li, V. Gupta, R. Singh, *J. Appl. Phys.* **2019**, *125*, 144501.

[41] T. Li, F. Wang, R. Lin, W. Xie, Y. Li, W. Zheng, F. Huang, *CrystEngComm* **2020**, *22*, 654.

[42] W. Zheng, R. Lin, D. Zhang, L. Jia, X. Ji, F. Huang, *Adv. Opt. Mater.* **2018**, *6*, 1800697.

[43] J. Yang, Y. Gao, W. Zheng, R. He, Z. Huo, X. Ji, *Cryst. Growth Des.* **2022**, *22*, 1731.